




# Encoding quantum bits in bound electronic states of a graphene nanotorus

J. Furtado <sup>1,\*</sup>, A. C. A. Ramos,<sup>1,†</sup> J. E. G. Silva,<sup>1,‡</sup> R. Bachelard <sup>2,3,§</sup> and Alan C. Santos <sup>2,4,¶</sup>

<sup>1</sup>Centro de Ciências e Tecnologia, Universidade Federal do Cariri, 63048-080, Juazeiro do Norte, Ceará, Brazil

<sup>2</sup>Departamento de Física, Universidade Federal de São Carlos, Rodovia Washington Luís, km 235 - SP-310, 13565-905 São Carlos, SP, Brazil

<sup>3</sup>Université Côte d'Azur, CNRS, Institut de Physique de Nice, 06560 Valbonne, France

<sup>4</sup>Department of Physics, Stockholm University, AlbaNova University Center 106 91 Stockholm, Sweden

(Dated: March 28, 2022)

We propose to use the quantum states of an electron trapped on the inner surface of a graphene nanotorus to realize as a new kind of physical quantum bit, which can be used to encode quantum information. Fundamental tasks for quantum information processing, such as the qubit initialization and the implementation of arbitrary single qubit gates, can be performed using external magnetic and electric fields. We also analyze the robustness of the device against systematic errors, which can be suppressed by a suitable choice of the external control fields. These findings open new prospects for the development of an alternative platform for quantum computing, for which the scalability remains to be determined.

## I. INTRODUCTION

Quantum bits (qubits) constitute the most fundamental unit of information for quantum computation, exploiting the properties of two-level systems to be in a superposition of quantum states. Considering the potential advantage of quantum computers in solving hard problems through quantum algorithms, such as Shor's [1, 2] and Simon's [3, 4] algorithms, efforts have been dedicated to identify suitable physical platforms to encode qubits. Qubits have been successfully encoded in degrees of freedom of light [5, 6], spins in nuclear magnetic resonance of atoms [7], spin in quantum dots [8], semiconductor spins [9], and trapped ions [10] among others [11]. Recently, impressive progresses have also been achieved with superconducting qubits [12, 13], driven by the interest of the community to proposing different kinds of physical qubits for quantum computation.

On the other hand, the outstanding properties of two-dimensional materials sparked a revolution in physical science. In particular, the features of curved graphene has been exploited to devise new electronic devices, such as helical strips with chiral effects, also known as chiraltronics [14–16], and Möbius strips with topological insulator properties [17]. Bridges connecting layers of graphene have also been proposed using a catenoid surface [18–20]. These curved materials are described by an effective Dirac Hamiltonian for a massless and gapless electron in the single layer of graphene [21], and the surface curvature is associated with a geometric potential, the so-called da Costa potential [22, 23]. Among the curved geometries of interest, the torus can be built by gluing the two edges of a nanotube, and presents a rich phenomenology [24–27]. In particular, it exhibits a number of bound states, whose spectrum and geometry can be manipulated with external electric and magnetic fields [28].

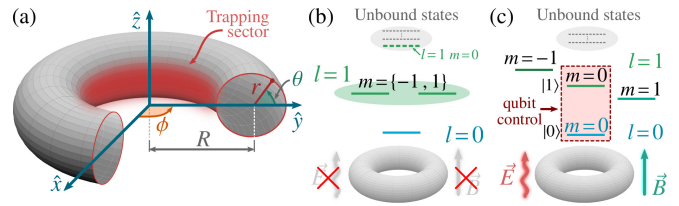


Figure 1. (a) Schematic representation of the nanotorus submitted to a static magnetic field (used to prepare the qubit) and to a time-dependent electric field (used to control the qubit and implement gates). The trapping sector in which the electron is confined is shown in green, for the orbital angular momentum  $m = 0$  states. (b) In absence of an external magnetic field, there exist a single bound state, with  $|l = 0, m = 0\rangle$ , and a pair of degenerate states  $|l = 1, m = \pm 1\rangle$ . (c) When applying an external magnetic field, the geometrical effects induce a Zeeman-like breaking of degeneracy of the states with  $l = 1$ , while a new bound state  $|l = 1, m = 0\rangle$ , used to realize our two-level system, arises.

In this paper we propose to encode a qubit in the quantum states of an electron confined on the surface of a graphene nanotorus, as sketched in Fig. 1. The curvature-induced trapping potential leads to a discrete set of quantum states, which are well characterized by two quantum numbers, namely, the total angular momentum  $l$  and its component along the quantization axis  $m$ . We also show how the qubit can be initialized, and how gates can be implemented. Furthermore, the robustness of such information processing against systematic errors is characterized, showing how they can be mitigated by external control fields. Considering the number of techniques to produce and probe such a nanotorus (and nanorings, a similar geometry) [24–27, 29–34], our proposal paves the way for the experimental realization of a new kind of qubit, under well-controlled conditions.

## II. THE SYSTEM AND FIRST QUANTIZATION

We here consider an electron confined on the surface of a nanotorus made of graphene, and it is characterized by the minor radius  $r$  and the major radius  $R$ , see Fig. 1a. Thanks to the

\* job.furtado@ufca.edu.br

† antonio.ramos@ufca.edu.br

‡ euclides.silva@ufca.edu.br

§ romain@ufscar.br

¶ ac.santos@df.ufscar.br

axial symmetry, the wavefunctions of the time-independent Schrödinger equation reduces to  $\psi_{n,l,m}(\theta, \phi) = \chi_{n,l}(\theta)e^{im\phi}$ , where  $\phi$  is the angle around the torus axis of revolution, and  $\theta$  the one around the tube. As we shall see,  $m$  is the quantum number associated with the component of the angular momentum in direction  $\hat{Z}$ , and the angular component of the wavefunction  $\chi_{n,l}(\theta)$  takes into account the quantum numbers related to the electronic energy level  $n$  and the total angular momentum of the system  $l$ . It satisfies the following time-independent Schrödinger equation [28]:

$$-\frac{\hbar^2}{2m^*r^2} \frac{d^2\chi(\theta)}{d\theta^2} + V_{\text{bare}}(\theta)\chi(\theta) = \epsilon\chi(\theta), \quad (1)$$

where the potential  $V_{\text{bare}}$  reads

$$V_{\text{bare}}(\theta) = \frac{\hbar^2}{2m^*r^2(R+r\cos\theta)^2} \left[ -\frac{R^2}{4} + r^2m^2 + \frac{r^2\sin^2\theta}{4} + \frac{r(R\cos\theta+r)}{2} \right], \quad (2)$$

with  $m^* = 0.3m_0$  the effective mass of the electron on the torus surface, and  $m_0$  is the rest mass of the electron [27]. Under a suitable choice of the parameters  $R$  and  $r$ , a single confined state exists, for which the probability density function reveals a “trapping sector” in the inner region of the nanotorus ( $\theta = \pi$ ). As highlighted in Fig. 1a, its width at half height is  $\delta\theta \approx \pi$ , so the electronic wavefunction forms a ring located around  $\theta = \pi$  [28].

However, in presence of external fields, whether electric or magnetic, the potential changes and  $V_{\text{bare}}$  in Eq. (1) must be substituted by the effective potential  $V(\theta) = V_{\text{bare}}(\theta) + V_E(\theta) + V_B(\theta)$ , in which  $V_E(\theta)$  and  $V_B(\theta)$  account for electric and magnetic field contributions, respectively:

$$V_E(\theta) = -eEr \sin\theta, \quad (3)$$

$$V_B(\theta) = \frac{e^2B^2}{8m^*}(R+r\cos\theta)^2 - \frac{me\hbar B}{2m^*}. \quad (4)$$

The Hamiltonian of the system in presence of electric and magnetic static fields then reads

$$H(\theta) = -\frac{\hbar^2}{2m^*r^2} \frac{d^2}{d\theta^2} + V(\theta). \quad (5)$$

These external fields can drastically alter the confinement potential of the electron on the surface of the nanotorus, resulting in new confined electronic near-ground states. In what follows, we focus on the set of states associated to the total angular momentum  $l = \{0, 1\}$ , since they are already suitable candidates to encode a quantum bit of information.

### A. Electronic near-ground states

In Fig. 2, we present the change in energy levels induced by the external magnetic field (from  $B = 0T$  to  $B = 0.45T$ ), with the lowest-lying states associated with  $l = \{0, 1\}$  represented. As sketched in Fig. 2a, by applying an external

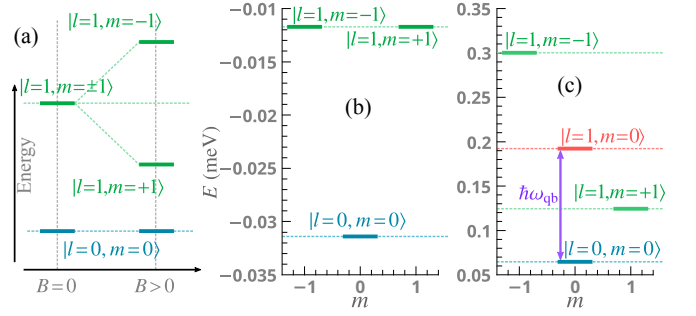


Figure 2. (a) Schematic representation of the Zeeman-like splitting. (b) Energy diagram of the three lowest-lying bound states of the system in absence of fields ( $B = 0T$ ), when the electron is subject only to the potential induced by curvature effects. (c) By turning on the magnetic field (here we set  $B = 0.45 T$ ), new bound states appear and a Zeeman-like splitting occurs, here stemming from both magnetic field and geometrical effects. This allows one to encode a bit of quantum information in the energy subspace spanned by the states  $l = \{0, 1, m = 0\}$ .

magnetic field the degenerate subspace  $\{|l = 1, m = \pm 1\rangle\}$  becomes non-degenerate. In the absence of magnetic field, the bound states correspond to  $|l = 0, m = 0\rangle$  and  $|l = 1, m = \pm 1\rangle$ , whereas the state  $|l = 1, m = 0\rangle$  is not bound. According to Eq. (2), the term  $r^2m^2$  leads to a degenerate subspace for the states  $\{|l = 1, m = \pm 1\rangle\}$ , illustrated in Fig. 2b. However, applying a strong magnetic field allows one to modify substantially the potential, so the state  $|l = 1, m = 0\rangle$  becomes bound and the last term in Eq. (4) lifts the degeneracy of the subspace  $\{|l = 1, m = \pm 1\rangle\}$ , see Fig. 2c.

We point out that when under the action of an electric field, the number of confined states also increases, and become spatially displaced over the nanotorus surface. Nevertheless, these states are doubly degenerate to  $m = \{\pm 1, \pm 2, \dots\}$ , a situation which is undesirable for the initialization of the qubit state. Indeed, degenerate states are not adequate for quantum information encoding, since multiple states may become populated. This motivates the choice of a static magnetic field over the nanotorus to build the qubit. In this context, we emphasize that the breaking of degeneracy by the magnetic field is different in nature from the Zeeman effect, in the sense that the field drastically modifies the geometric potential, in addition to shifting the energy of the associated levels.

## III. ELECTRONIC QUBIT ENCODING

Let us adopt DiVincenzo’s approach to characterize our system as a qubit suitable to encode quantum information [35], focusing on the two following criteria: (1) *A physical system (1) with well characterized qubit (i.e., two-level system), and (2) which can be coherently controlled, is a candidate for quantum information processing.* The additional DiVincenzo’s criteria concern the scalability, decoherence effects and the readability of the quantum information encoded in the qubits, which we discuss only briefly in the conclusions.

We first consider the case when an external magnetic field

is applied over the system and the orbital angular momentum  $m$  is taken to be zero. The  $m = 0$  states are often considered, for example, in quantum computing with trapped ions [36–39]. Returning to Eq. (5) and doing an expansion around the trapping region ( $\theta \approx \pi$ ), one obtains

$$V_{\text{bare}}(\theta_\pi) + V_B(\theta_\pi) = \frac{\beta^2}{2m^*} \theta_\pi^2 + \delta \theta_\pi^4 + \epsilon, \quad (6)$$

where we have introduced the variable  $\theta_\pi = \theta - \pi$ . The coefficients  $\beta$ ,  $\delta$  and  $\epsilon$  are given by

$$\delta = -\frac{1}{96m^*} \left[ \frac{\hbar^2 r(R+8r)}{(R-r)^4} + e^2 B^2 r(R-4r) \right], \quad (7a)$$

$$\beta^2 = \frac{r}{4} \left[ \frac{\hbar^2}{(R-r)^3} + e^2 B^2 (R-r) \right], \quad (7b)$$

$$\epsilon = \frac{1}{8m^*(R-r)^2} \left[ e^2 B^2 (R-r)^4 - \frac{\hbar^2 (R^2 - 2Rr + 2r^2)}{r^2} \right]. \quad (7c)$$

The first quantization is realized by identifying the canonical variables of position,  $\theta_\pi \rightarrow \hat{\theta}_\pi$ , and momentum  $\hat{p}_\theta = (i/r)d(\bullet)/d\theta_\pi$ , as operators. In this first-quantization picture, the Hamiltonian of the system now reads

$$\hat{H}_0 = -\frac{\hbar^2}{2m^*r^2} \frac{d^2}{d\hat{\theta}_\pi^2} + \epsilon + \frac{\beta^2}{2m^*} \hat{\theta}_\pi^2 + \delta \hat{\theta}_\pi^4. \quad (8)$$

This Hamiltonian describes a modified harmonic potential with anharmonicity  $\delta$ , which is reminiscent of the one obtained for superconducting qubits [40–43]. In particular, the change of variables  $\hat{\theta}_\pi \rightarrow \hat{q}/r$  leads to

$$\hat{H}_0 = \frac{\hat{p}^2}{2m^*} + \frac{m^* \omega^2}{2} \hat{q}^2 + \frac{\delta}{r^4} \hat{q}^4 + \epsilon \mathbb{1}. \quad (9)$$

The connection with artificial superconducting atoms is made more straightforward by defining the creation and annihilation operators,  $\hat{a}^\dagger = (\hat{q} - id/d\hat{q})/\sqrt{2}$  and  $\hat{a} = (\hat{q} + id/d\hat{q})/\sqrt{2}$  respectively, so we obtain the anharmonic oscillator Hamiltonian:

$$\hat{H}_0 = \mathbb{1}E_0 + \hbar\omega \hat{a}^\dagger \hat{a} + \delta \left( \frac{\hbar}{2m^* \omega r^2} \right)^2 (\hat{a} + \hat{a}^\dagger)^4, \quad (10)$$

with  $E_0 = \epsilon + \hbar\omega/2$  and  $\omega = |\beta|/m^*r$ . The first two terms correspond to the quantum harmonic oscillator with ground-state energy  $E_0$  and a spectrum of energies separated by quanta of energy  $\hbar\omega$ . The third term of the above equation stands for the anharmonicity parameter. We hereafter refer to this Hamiltonian as our *bare Hamiltonian*, which defines the typical properties of our system, such as the qubit energy scale and qubit transition frequency.

As an alternative to genuine two-level systems, such as spin and photon polarization qubits, one can exploit the large anharmonicity to induce energy shifts in the upper-excited levels, so the system operates effectively as a two-level system. Indeed, when driving the lowest excited state, the probability to gain a second quantum of energy is negligible. This

scheme is often used in artificial atoms, such as in superconducting qubits [42, 43]. In the case of the nanotorus, increasing the external magnetic field  $B$  allows one to produce an effective two-level system which spans the subspace  $\mathcal{S}_{\text{qb}} = \{|l=0, m=0\rangle, |l=1, m=0\rangle\}$ , with the main quantum number  $m=0$  and  $l=\{0,1\}$ , see Fig. 2. Now assuming that the system only explores the two energy levels of  $\mathcal{S}_{\text{qb}}$ , the bosonic operators  $\hat{a}$  and  $\hat{a}^\dagger$  can be substituted by  $\hat{\sigma}_-$  and  $\hat{\sigma}_+$ , respectively, the Pauli matrices defined as  $\hat{\sigma}_- = |l=0, m=0\rangle\langle l=1, m=0|$  and  $\hat{\sigma}_+ = (\hat{\sigma}_-)^\dagger$ . The Hamiltonian for the qubit then reads

$$\hat{H}_{\text{qb}} = \hbar\omega \hat{\sigma}_+ \hat{\sigma}_- + \alpha (\hat{\sigma}_+ + \hat{\sigma}_-)^4 + \mathbb{1}E_0, \quad (11)$$

with  $\alpha = \delta(\hbar/2m^* \omega r^2)^2$ . Moreover, since the second term in the above equation can be rewritten as  $\alpha(\hat{\sigma}_+ + \hat{\sigma}_-)^4 = \alpha \mathbb{1}$ , we simplify the above Hamiltonian by redefining the zeroth energy level to get

$$\hat{H}_{\text{qb}} = \hbar\omega \hat{\sigma}_+ \hat{\sigma}_-. \quad (12)$$

We stress that this Hamiltonian is valid only when transitions occur only inside the subspace  $\mathcal{S}_{\text{qb}}$ , where no change in the main quantum number is promoted. With a stronger magnetic field, new bound states with  $m=0$  will appear, so the system will turn in an effective multilevel atom.

#### IV. QUBIT INITIALIZATION AND CONTROL

As mentioned before, when the magnetic field is below a certain value  $B_{\text{ini}}$ , hereafter called initialization static magnetic field, the system presents a single low-lying state for which  $m=0$ . The others states have a number  $m \neq 0$ , as illustrated in Fig. 2. In this case, an electron trapped in the nanotorus tends to populate this specific state, since it has the lowest energy. The qubit initialization is then achieved by introducing an external magnetic field which is strong enough to turn the electronic state  $|l=1, m=0\rangle$  into a bound state, but not too strong so that the subspace corresponding to  $m=0$  contains only two states. Hence, the system behaves as an effective two-level system. Since the system has previously been initialized in the state  $|l=0, m=0\rangle$ , and since the magnetic field variation does not promote any transition, the system remains in the state  $|\psi(0)\rangle = |l=0, m=0\rangle$ , which concludes the initialization of the qubit.

In Fig. 3, we present the energy of the bound states as a function of the magnetic field, showing the value of  $B_{\text{min}}$  and  $B_{\text{max}}$  for two different values of the external radius  $R$ . Indeed, the precise range of values for the magnetic field required to initialize the qubit depends on the specific geometry of the nanotorus, through the minor  $r$  and major radius  $R$ .

##### A. Qubit control and universal single-qubit quantum gates

As for the majority of quantum emitters, the driving of a specific transition can be achieved using an external electric field, using a local field to control the qubit. Introducing the

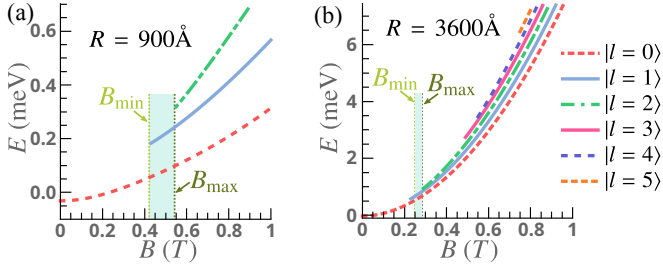


Figure 3. Energy levels (with  $m = 0$ ) of an electron confined on the inner radius of a nanotorus as function of the external magnetic field  $B$  (in Tesla) for two configurations: (a)  $r = 350\text{\AA}$  and  $R = 900\text{\AA}$ , and for (b)  $r = 350\text{\AA}$  and  $R = 3600\text{\AA}$ . In both cases, the first and second curves, from bottom to top, correspond to the fundamental level  $|l = 0, m = 0\rangle$  and first excited one  $|l = 1, m = 0\rangle$ , respectively. The other curves correspond to other energy levels, which are undesirable in the present scheme to encode a qubit.

electric field  $\vec{E} = E\hat{Z}$  manifests, in Hamiltonian (5), in an additional contribution:  $\hat{H} = \hat{H}_0 + \hat{H}_E$ , with

$$\hat{H}_E = erE \sqrt{\frac{\hbar}{2r|\beta|}} \left[ (\hat{a} + \hat{a}^\dagger) - \frac{\hbar}{12r|\beta|} (\hat{a} + \hat{a}^\dagger)^3 \right]. \quad (13)$$

Considering again an external magnetic field such that we have only the low-lying states  $|n\rangle = |l = n, m = 0\rangle$ , we can replace the operators  $\hat{a}$  and  $\hat{a}^\dagger$  by  $\hat{\sigma}_-$  and  $\hat{\sigma}_+$  in Eq. (13), which leads to

$$\hat{H}_E = \hbar\Omega(E)(\hat{\sigma}_+ + \hat{\sigma}_-). \quad (14)$$

We have used that  $(\hat{\sigma}_- + \hat{\sigma}_+)^3 = (\hat{\sigma}_- + \hat{\sigma}_+)$  and introduced the frequency  $\Omega(E) = \mu E/\hbar$ , with  $\mu$  a parameter given by

$$\mu = er \left[ \sqrt{\frac{\hbar}{2r|\beta|}} - \frac{1}{6} \left( \sqrt{\frac{\hbar}{2r|\beta|}} \right)^3 \right]. \quad (15)$$

Since the quantity  $\hbar/r|\beta|$  is dimensionless,  $\mu$  has dimension of a ‘charge-distance’, i.e., the dimension of an electric dipole moment (see Appendix A for further details). Furthermore, the amplitude of  $\Omega(E)$  here depends on both the electric and magnetic fields, in addition to other parameters related to the system geometry. The controllability of the system is thus strongly related to the control of the driving electric field  $E$ , once the other parameters have been fixed. In particular, by considering a time-dependent oscillating radio-frequency (RF) field  $E$  given by

$$E = E_0 \cos(\omega_{\text{rf}}t + \phi), \quad (16)$$

with  $\phi$  an adjustable phase, the driving Hamiltonian becomes

$$H_{\text{dv}}(t) = \hbar\omega\sigma^+\sigma^- + \hbar\Omega(E_0) \cos(\omega_{\text{rf}}t + \phi)(\sigma^+ + \sigma^-). \quad (17)$$

As a final step, let us derive the system effective dynamics, close to resonance. According to Schrödinger equation, the system evolves as

$$i\hbar |\dot{\psi}(t)\rangle = H_{\text{dv}}(t) |\psi(t)\rangle, \quad (18)$$

since no external dissipative channel is taken into account. In order to explore the two-level nature of the system, we then consider the case of a resonant driving ( $\Omega(E_0) \ll \omega$ ). Furthermore, we move to the rotating frame of the external field, consider the Rotating Wave Approximation, so the dynamics of the system is dictated by the driving effective Hamiltonian (see Appendix B)

$$H_{\text{eff}} = \hbar\Delta\sigma_+\sigma_- + \frac{\hbar\Omega(E_0)}{2} (e^{i\phi}\sigma_- + e^{-i\phi}\sigma_+), \quad (19)$$

where  $\Delta = \omega - \omega_{\text{rf}}$  is the detuning between the qubit transition frequency and the external field frequency. The above Hamiltonian, where the phase  $\phi$  is controlled through the driving field, can then be used to implement *arbitrary* single qubit gates [44], so one can conclude that the di Vincenzo’s criteria to use a physical qubit for quantum computation are fulfilled.

## B. Preparation of an arbitrary input state

In this section we show how to choose adequately the parameters of the effective Hamiltonian  $H_{\text{eff}}$  in order to prepare an arbitrary input state given by

$$|\psi(\theta, \eta)\rangle = \sin(\theta/2)|0\rangle + e^{i\eta} \cos(\theta/2)|1\rangle, \quad (20)$$

for any  $\theta \in (0, \pi]$  and  $\eta \in [0, \pi]$ . The system is initially prepared in the state  $|0\rangle$  using the procedure discussed previously. Then, using a resonant RF field ( $\omega_{\text{rf}} = \omega$ ), the system evolves toward  $|\Psi(t, \phi)\rangle = e^{-\frac{i}{\hbar}H_{\text{eff}}t}|0\rangle$ , which reads

$$|\Psi(t, \phi)\rangle = \cos\left(\frac{t\Omega}{2}\right)|0\rangle + e^{-i(\phi+\frac{\pi}{2})} \sin\left(\frac{t\Omega}{2}\right)|1\rangle. \quad (21)$$

By comparing the above equation with Eq. (20), it becomes clear the total evolution time and the phase  $\phi$  can be chosen to achieve any state of the form (20). As an illustration, we show in Fig. 4a the trajectory of the quantum state on the Bloch sphere, driven by Hamiltonian (19). After initializing the system in the state  $|0\rangle$ , we set the total evolution time as  $\tau = \pi/2\Omega$  such that the final state is one of the set of quantum states  $\mathcal{E}$  at the equator of the Bloch sphere, which is a set of states with maximum quantum coherence in basis  $\{|0\rangle, |1\rangle\}$  [45]. That is, the set  $\mathcal{E}$  of all states of the form  $|\xi(\eta)\rangle = (|0\rangle + e^{i\eta}|1\rangle)/\sqrt{2}$ . Hence, by tuning the parameter  $\phi$ , we can prepare any state in  $\mathcal{E}$ . In Fig. 4b, we show sequential steps of the implementation for each evolution considered in Fig. 4a. In Fig. 4c the equivalent quantum circuit where a Hadamard and phase gate are implemented, two genuine quantum gates which do not have an equivalent in classical computation [11].

## V. SYSTEMATIC ERRORS AND GATE FIDELITY

When the external fields used to qubit initialization and control present fluctuations around a reference value, it directly affects the qubit control in different ways. In this section we study the performance of the gate implementation in

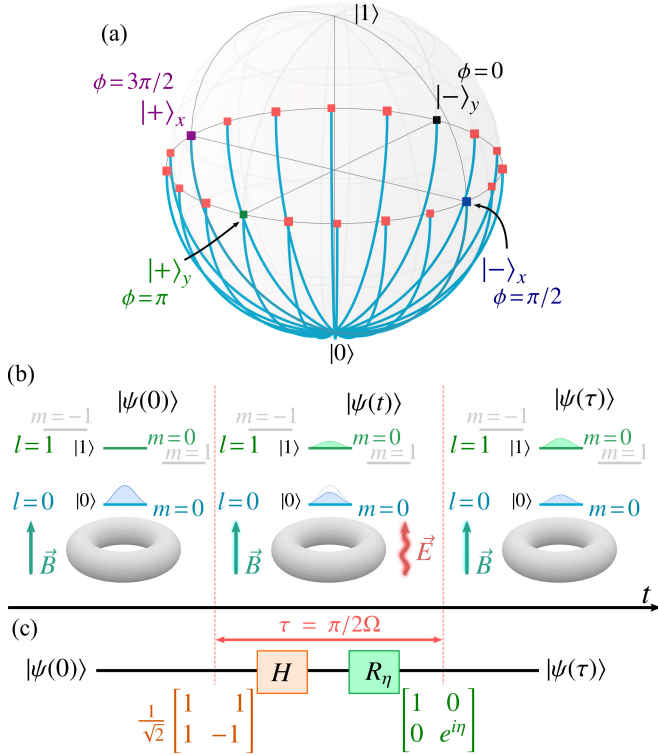


Figure 4. (a) Trajectories on the Bloch sphere obtained for different choices of the parameter  $\phi$ . The total evolution time  $\tau = \pi/2\Omega$  brings the system to one of the state in the equator of the sphere, where any state in  $\mathcal{E}$  can be prepared. The states in the  $x$ - and  $y$ -axis of the Bloch sphere are defined as  $|\pm\rangle_x = (|0\rangle \pm |1\rangle)/\sqrt{2}$  and  $|\pm\rangle_y = (|0\rangle \pm i|1\rangle)/\sqrt{2}$ . (b) Schematic representation of each step in the implementation of the quantum circuit shown in (c), where a magnetic field is used to initialize the system in the ground state  $|0\rangle$ , followed by the coherent control using the external electric field which drives the system to a desired final state. In (c) we show the quantum gates Hadamard ( $H$ ) and phase gate ( $R_\eta$ ), satisfying  $H|n\rangle = (|0\rangle + (-1)^n|1\rangle)/\sqrt{2}$ , with  $n \in \{0, 1\}$ , and  $R_\eta(a|0\rangle + b|1\rangle) = a|0\rangle + be^{i\eta}|1\rangle$ .

presence of systematic errors. In our system, according to Eqs. (7), (15) and (19), fluctuations in the magnetic field have an impact on the qubit energy (and thus on its frequency) and on the effective electric dipole moment. On the other hand, any error associated to the electric field amplitude only affects the control of the qubit.

We consider an analysis of the systematic error based on the deviation between a desired quantum gate  $G$  (target unitary operation) and the real operation implemented through the perturbed Hamiltonian. We call the unperturbed and perturbed Hamiltonians  $H_{\text{eff}}$  and  $H_{\text{per}} = H_{\text{per}}(\delta B, \delta E)$ , respectively, where  $\delta B$  and  $\delta E$  encode the fluctuations of the magnetic and electric fields, respectively. We then let the system evolves under the action of  $H_{\text{per}}$  and compare the outcome state  $|\psi_{\text{eff}}\rangle$  with the state  $|\psi_{\text{per}}\rangle$  expected when we drive the system with  $H_{\text{eff}}$  during the time interval  $\Delta t$  necessary to im-

plement the gate. Given the evolution operators

$$U_{\text{eff/per}}(\Delta t) = \exp\left(\frac{1}{i\hbar}H_{\text{eff/per}}\Delta t\right), \quad (22)$$

where the unperturbed dynamics gives  $U_{\text{eff}}(\Delta t) = G$ , we compute the infidelity as given by the Bures metric for pure states [46]

$$\mathcal{F}(|\psi_{\text{eff}}\rangle, |\psi_{\text{per}}\rangle) = 1 - |\langle\psi_{\text{eff}}|\psi_{\text{per}}\rangle|^2, \quad (23)$$

with  $|\psi_{\text{eff/per}}\rangle = U_{\text{eff/per}}(\Delta t)|\psi_{\text{input}}\rangle$  and  $|\psi_{\text{input}}\rangle$  an arbitrary input state. Since we need to implement single qubit gates to arbitrary input states, the error analysis is realized using the average over many input states of a given operation. We implement each dynamics and take the average of  $\mathcal{F}(|\psi_{\text{eff}}\rangle, |\psi_{\text{per}}\rangle)$  over  $N$  random input states  $|\psi_{\text{input}}\rangle$ .

Let us here consider the average infidelity to implement the Hadamard gate as a function of the deviation amplitude of the magnetic field  $\delta B/B_0$ , where  $B_0$  is a reference value. From the maximum deviation we estimated the fluctuations in the final state from the relation  $\delta\mathcal{F} = \max_{|\psi_{\text{inp}}\rangle} \mathcal{F}(|\psi_{\text{eff}}\rangle, |\psi_{\text{per}}\rangle)$ . In Fig. 5a we show the behaviour of the infidelity with respect to  $\delta B/B_0$  for two different values of magnetic field  $B_0$ . In the cases considered here, small deviations in  $B_0$  (less than 1%) are enough to promote a significant in the gate implementation. Note that errors of this magnitude are within reach of several experiments [47, 48], especially in state-of-the-art setups [49–51], where the control over the magnetic field is of order of  $\mu\text{T}$ . However, as shown in Fig. 5b, the negative effects induced by the fluctuations of the magnetic field can be mitigated by a suitable choice of the electric field, which sets the time of the gate implementation. In the case where the fluctuations are present in the electric field, with a relative error amplitude of  $\delta E/E_0$  around the reference value  $E_0$ , the qubit control is much more robust to errors than for a fluctuating  $B_0$  see Figs. 5c and 5d. However, our results suggest the magnetic field, within the values presented in 3b, does not allow to reduce the effects of the fluctuating electric field.

## VI. CONCLUSIONS AND PROSPECTS

In this paper we have introduced a new kind of physical two-level system which can be used to process quantum information. In particular, we showed that the curvature of a graphene surface induces a confining potential for an electron. The electronic energy level structure is suitable to the encoding of quantum information as a superposition of the two lowest energy states  $|l = \{0, 1\}, m = 0\rangle = ||0, 1\rangle$ , and arbitrary single-qubit states in the form  $|\psi\rangle = a|0\rangle + b|1\rangle$  can be prepared and manipulated through external magnetic and electric fields. Our system obeys the DiVincenzo's criteria that states that any new proposal of qubit must allow for a perfect encoding of information and a coherent control of information. As a first analysis of errors in such a system, we quantified how undesired fluctuations in magnetic and electric field may affect the gate fidelity. As a proposal to partially suppress such effects, we showed an optimization scheme that

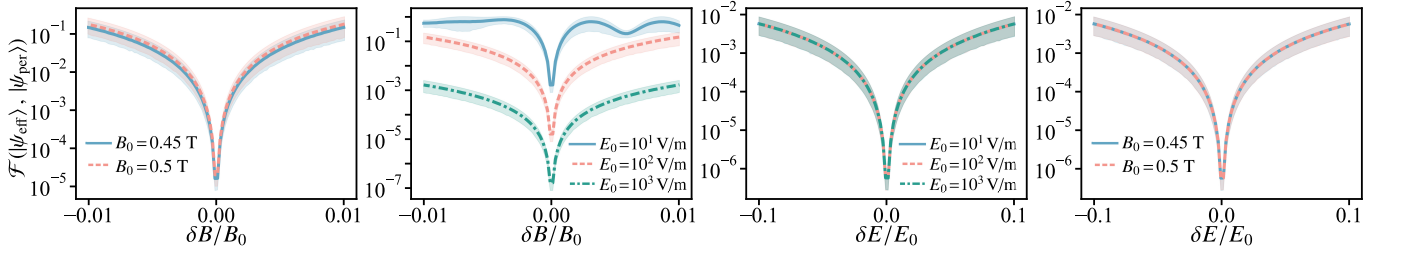


Figure 5. (a) Average infidelity of the Hadamard gate under systematic errors in magnetic field over  $N = 10,000$  random input states, for different values of  $B_0$ . We set  $E_0 = 100$  V/m. (b) By choosing the electric field amplitude in an adequate way, gate error mitigation is possible. In our example we use  $B_0 = 0.45$  T. (c) Average infidelity for errors in the electric field for different values of  $E_0$ , where we choose  $B_0 = 0.45$  T. (d) By changing the magnetic field inside the limit imposed in Fig. 3a, no enhancement is observed. Here we set  $E_0 = 1,000$  V/m. In all graphs we used the parameters considered in Fig. 3a.

explores an adequate choice in amplitude of the electric field used to implement single-qubit gates.

It is timely to say that any proposal of quantum computer begins with a proposal of highly controllable single qubits. However, the scalability and selective controllability of multi-qubit gates are other fundamental requirements in DiVincenzo's view [35]. In particular, a system able to implement arbitrary single-qubit gates and any entangling two-qubit gate (such as the CNOT, or controlled flip phase gate) is eligible as a device able to perform universal quantum computation [52]. In our system, building a two-qubit system is, in principle, possible due to the recent progress in the production and control of multiple organic nanorings [30–32], along with progress on their realization on a larger scale [33]. Moreover, understanding the influence of the environment over the system, and thus decoherence effects [53], is a fundamental issue which remains to be addressed. Due to the coupling of electrons with the phonon modes in graphene [54–59], in addition to the hot-electron relaxation [60] and curvature effects [61, 62], the environment is bound to exert an influence over the computational performance of our system. In this sense, our results should not be understood as the whole story, but rather as the initial step of a long and challenging path towards a new potential platform for quantum computation.

## ACKNOWLEDGMENTS

R.B. and A.C.S. are supported by the São Paulo Research Foundation (FAPESP) through Grants Nos. 2019/22685-1, 2019/13143-0, 2018/15554-5 and 2021/10224-0. R.B. received support from the National Council for Scientific and Technological Development (CNPq) Grant Nos. 313886/2020-2 and 409946/2018-4.

### Appendix A: Dimensional analysis of Eq. (15)

Let us consider

$$\mu_0 = er \left[ \sqrt{\frac{\hbar}{2r|\beta|}} - \frac{1}{2} \left( \sqrt{\frac{\hbar}{2r|\beta|}} \right)^3 \right]. \quad (\text{A1})$$

where the dimensional analysis of  $\beta$  follows

$$\begin{aligned} |\beta| &= \sqrt{[r] \left[ \frac{[\hbar]^2}{[(R-r)^3]} + [e]^2 [B]^2 [(R-r)] \right]} \\ &= \sqrt{m \left[ \frac{(J \cdot s)^2}{m^3} + C^2 T^2 m \right]} = \sqrt{\frac{J^2 \cdot s^2}{m^2} + C^2 \frac{Kg^2}{C^2 \cdot s^2} m^2} \\ &= \sqrt{\frac{J^2 \cdot s^2}{m^2} + \frac{Kg^2}{s^2} m^2} = \sqrt{\frac{Kg^2 \cdot m^4 \cdot s^2}{s^4 \cdot m^2} + \frac{Kg^2}{s^2} m^2} \\ &= \sqrt{\frac{Kg^2 \cdot m^2}{s^2}} = \frac{Kg \cdot m}{s} \end{aligned} \quad (\text{A2})$$

such that

$$\begin{aligned} \frac{[\hbar]}{[r][|\beta|]} &= \frac{J \cdot s}{m} \frac{s}{Kg \cdot m} = J \frac{s^2}{Kg \cdot m^2} \\ &= \frac{Kg \cdot m^2}{s^2} \frac{s^2}{Kg \cdot m^2} = 1, \end{aligned} \quad (\text{A3})$$

therefore we get

$$[\mu_0] = [e][r] = C \cdot m, \quad (\text{A4})$$

the dimension of electric dipole moment.

### Appendix B: Effective dynamics

Consider the total Hamiltonian  $H(t) = H_0 + H_1(t)$ , in which  $H_0 = \hbar\omega\sigma_+\sigma_-$ , as

$$H(t) = \hbar\omega\sigma_+\sigma_- + \hbar\Omega(E_0) \cos(\omega_{\text{rf}}t + \phi) (\sigma_- + \sigma_+). \quad (\text{B1})$$

Since in the above equation we have an small highly oscillating term, it is convenient to identify how to approximate it to an effective Hamiltonian using the Rotating Wave Approximation (RWA). To this end, we write the Schrödinger equation in the interaction picture using the transformation  $|\psi_1(t)\rangle = e^{iH_0 t/\hbar} |\psi(t)\rangle$  we get the dynamics for  $|\psi_1(t)\rangle$  as

$$i\dot{|\psi_1(t)\rangle} = i\hbar V_1(t) |\psi_1(t)\rangle, \quad (\text{B2})$$

with  $V_I(t) = e^{iH_0t/\hbar}H_1(t)e^{-iH_0t/\hbar}$ . As a first remark, note that  $[H_1(t_1), H_1(t_2)] = [V_I(t_1), V_I(t_2)] = 0$  for any  $(t_1, t_2)$ . It allows to write the solution for the system dynamics as

$$|\psi_I(t)\rangle = U_I(t)|\psi_I(0)\rangle, \quad (\text{B3})$$

with

$$U_I(t) = \exp\left[\frac{1}{i\hbar} \int_0^t V_I(\xi)d\xi\right]. \quad (\text{B4})$$

We use that

$$\begin{aligned} V_I(t) &= e^{iH_0t/\hbar}H_1(t)e^{-iH_0t/\hbar} \\ &= \frac{\hbar\Omega(E_0)}{2} \left( e^{i(\omega_{\text{rf}}t+\phi)} + e^{-i(\omega_{\text{rf}}t+\phi)} \right) e^{iH_0t/\hbar}(\sigma_+ + \sigma_-)e^{-iH_0t/\hbar} \\ &= \frac{\hbar\Omega(E_0)}{2} \left[ \left( e^{i(\omega_-t+\phi)} + e^{-i(\omega_+t+\phi)} \right) \sigma_- + \text{H.c.} \right], \end{aligned} \quad (\text{B5})$$

where  $\omega_{\pm} = \omega_{\text{rf}} \pm \omega$  and ‘H.c.’ denotes the Hermitian conjugate. Therefore, by integrating the above expression

$$\begin{aligned} \int_0^t V_I(\xi)d\xi &= \frac{i\hbar\Omega(E_0)}{2} \left[ \frac{e^{-i\phi} \left( e^{-i\omega_+t} - 1 \right)}{\omega_+} - \frac{e^{i\phi} \left( e^{i\omega_-t} - 1 \right)}{\omega_-} \right] \sigma_- \\ &+ \frac{i\hbar\Omega(E_0)}{2} \left[ \frac{e^{-i\phi} \left( e^{-i\omega_-t} - 1 \right)}{\omega_-} - \frac{e^{i\phi} \left( e^{i\omega_+t} - 1 \right)}{\omega_+} \right] \sigma_+. \end{aligned} \quad (\text{B6})$$

Thus, for a highly oscillating external field, we can approximate the above expression to

$$\int_0^t V_I(\xi)d\xi \approx \frac{\hbar\Omega(E_0)}{2} \left[ \frac{-ie^{i\phi} \left( e^{i\omega_-t} - 1 \right)}{\omega_-} \sigma_- + \text{H.c.} \right]. \quad (\text{B7})$$

For this reason, in our analysis we can neglect highly oscillating terms. In this case, we follow by writing the Hamiltonian  $H(t)$  in the rotating frame by using  $R(t) = e^{i\omega_{\text{rf}}t\sigma_+ \sigma_-}$ , such that we find

$$\begin{aligned} H_R &= R(t)H(t)R^\dagger(t) + i\hbar\dot{R}(t)R^\dagger(t) = \hbar\Delta\sigma_+\sigma_- + R(t)H_I(t)R^\dagger(t) \\ &= \hbar\Delta\sigma_+\sigma_- + \frac{\hbar\Omega(E_0)}{2} \left( e^{i(\omega_{\text{rf}}t+\phi)} + e^{-i(\omega_{\text{rf}}t+\phi)} \right) e^{-i\omega_{\text{rf}}t} \sigma_- + \text{H.c.}, \end{aligned} \quad (\text{B8})$$

where we define  $\Delta = \omega - \omega_{\text{rf}}$ . Now, by neglecting the highly oscillating terms  $e^{\pm 2i\omega_{\text{rf}}t}$ , it is possible to proof that we get

$$H_R = \hbar\Delta\sigma_+\sigma_- + \frac{\hbar\Omega(E_0)}{2} \left( e^{i\phi}\sigma_- + e^{-i\phi}\sigma_+ \right). \quad (\text{B9})$$

- 
- [1] P. Shor, in *Proceedings 35th Annual Symposium on Foundations of Computer Science* (1994) pp. 124–134.
- [2] P. W. Shor, “Polynomial-time algorithms for prime factorization and discrete logarithms on a quantum computer”, *SIAM Journal on Computing* **26**, 1484 (1997).
- [3] D. Simon, in *Proceedings 35th Annual Symposium on Foundations of Computer Science* (1994) pp. 116–123.
- [4] D. R. Simon, “On the power of quantum computation”, *SIAM J. Comput.* **26**, 1474–1483 (1997).
- [5] E. Knill, R. Laflamme, and G. J. Milburn, “A scheme for efficient quantum computation with linear optics”, *nature* **409**, 46 (2001).
- [6] P. Kok, W. J. Munro, K. Nemoto, T. C. Ralph, J. P. Dowling, and G. J. Milburn, “Linear optical quantum computing with photonic qubits”, *Rev. Mod. Phys.* **79**, 135 (2007).
- [7] I. Oliveira, R. Sarthour Jr, T. Bonagamba, E. Azevedo, and J. C. Freitas, *NMR quantum information processing* (Elsevier, Oxford, UK, 2011).
- [8] D. Loss and D. P. DiVincenzo, “Quantum computation with quantum dots”, *Phys. Rev. A* **57**, 120 (1998).
- [9] L. M. K. Vandersypen and M. A. Eriksson, “Quantum computing with semiconductor spins”, *Physics Today* **72**, 38 (2019).
- [10] J. I. Cirac and P. Zoller, “Quantum computations with cold trapped ions”, *Phys. Rev. Lett.* **74**, 4091 (1995).
- [11] M. A. Nielsen and I. L. Chuang, *Quantum Computation and Quantum Information: 10th Anniversary Edition*, 10th ed. (Cambridge University Press, New York, NY, USA, 2011).
- [12] F. Arute, K. Arya, R. Babbush, D. Bacon, J. C. Bardin, R. Barends, R. Biswas, S. Boixo, F. G. S. L. Brandao, D. A. Buell, B. Burkett, Y. Chen, Z. Chen, B. Chiaro, R. Collins, W. Courtney, A. Dunsworth, E. Farhi, B. Foxen, A. Fowler, C. Gidney, M. Giustina, R. Graff, K. Guerin, S. Habegger, M. P. Harrigan, M. J. Hartmann, A. Ho, M. Hoffmann, T. Huang, T. S. Humble, S. V. Isakov, E. Jeffrey, Z. Jiang, D. Kafri, K. Kechedzhi, J. Kelly, P. V. Klimov, S. Knysh, A. Korotkov, F. Kostritsa, D. Landhuis, M. Lindmark, E. Lucero, D. Lyakh, S. Mandrà, J. R. McClean, M. McEwen, A. Megrant, X. Mi, K. Michielsen, M. Mohseni, J. Mutus, O. Naaman, M. Neeley, C. Neill, M. Y. Niu, E. Ostby, A. Petukhov, J. C. Platt, C. Quintana, E. G. Rieffel, P. Roushan, N. C. Rubin, D. Sank, K. J. Satzinger, V. Smelyanskiy, K. J. Sung, M. D. Trevithick, A. Vainsencher, B. Villalonga, T. White, Z. J. Yao, P. Yeh, A. Zalcman, H. Neven, and J. M. Martinis, “Quantum supremacy using a programmable superconducting processor”, *Nature* **574**, 505 (2019).
- [13] Y. Wu, W.-S. Bao, S. Cao, F. Chen, M.-C. Chen, X. Chen, T.-H. Chung, H. Deng, Y. Du, D. Fan, M. Gong, C. Guo, C. Guo, S. Guo, L. Han, L. Hong, H.-L. Huang, Y.-H. Huo, L. Li, N. Li, S. Li, Y. Li, F. Liang, C. Lin, J. Lin, H. Qian, D. Qiao, H. Rong, H. Su, L. Sun, L. Wang, S. Wang, D. Wu, Y. Xu, K. Yan, W. Yang, Y. Yang, Y. Ye, J. Yin, C. Ying, J. Yu, C. Zha, C. Zhang, H. Zhang, K. Zhang, Y. Zhang, H. Zhao, Y. Zhao, L. Zhou, Q. Zhu, C.-Y. Lu, C.-Z. Peng, X. Zhu, and J.-W. Pan, “Strong quantum computational advantage using a superconducting quantum processor”, *Phys. Rev. Lett.* **127**, 180501 (2021).
- [14] R. Dandoloff and T. Truong, “Quantum hall-like effect on strips due to geometry”, *Physics Letters A* **325**, 233 (2004).

- [15] V. Atanasov, R. Dandoloff, and A. Saxena, “Geometry-induced charge separation on a helicoidal ribbon”, *Phys. Rev. B* **79**, 033404 (2009).
- [16] V. Atanasov and A. Saxena, “Helicoidal graphene nanoribbons: Chiraltronics”, *Phys. Rev. B* **92**, 035440 (2015).
- [17] Z. L. Guo, Z. R. Gong, H. Dong, and C. P. Sun, “Möbius graphene strip as a topological insulator”, *Phys. Rev. B* **80**, 195310 (2009).
- [18] R. Dandoloff, “Quantum anticentrifugal force for wormhole geometry”, *Physics Letters A* **373**, 2667 (2009).
- [19] R. Dandoloff, A. Saxena, and B. Jensen, “Geometry-induced potential on a two-dimensional section of a wormhole: Catenoid”, *Phys. Rev. A* **81**, 014102 (2010).
- [20] J. Silva, J. Furtado, T. Santiago, A. C. Ramos, and D. da Costa, “Electronic properties of bilayer graphene catenoid bridge”, *Physics Letters A* **384**, 126458 (2020).
- [21] M. I. Katsnelson, *Graphene: Carbon in Two Dimensions* (Cambridge University Press, 2012).
- [22] R. C. T. da Costa, “Quantum mechanics of a constrained particle”, *Phys. Rev. A* **23**, 1982 (1981).
- [23] R. C. T. da Costa, “Constraints in quantum mechanics”, *Phys. Rev. A* **25**, 2893 (1982).
- [24] M. Ahlskog, E. Seynaeve, R. Vullers, C. Van Haesendonck, A. Fonseca, K. Hernadi, and J. B. Nagy, “Ring formations from catalytically synthesized carbon nanotubes”, *Chemical Physics Letters* **300**, 202 (1999).
- [25] X. Wang, Z. Wang, Y. qi Liu, C. Wang, C. Bai, and D. Zhu, “Ring formation and fracture of a carbon nanotube”, *Chemical Physics Letters* **339**, 36 (2001).
- [26] R. Martel, H. R. Shea, and P. Avouris, “Ring formation in single-wall carbon nanotubes”, *J. Phys. Chem. B* **1999**, 103, 36, 7551–7556 **103**, 7551 (1999).
- [27] R. Haddon, “Electronic properties of carbon toroids”, *Nature* **388**, 31 (1997).
- [28] J. E. G. Silva, J. Furtado, and A. C. A. Ramos, “Electronic properties of a graphene nanotorus under the action of external fields”, *The European Physical Journal B* **93**, 225 (2020).
- [29] H. Omachi, T. Nakayama, E. Takahashi, Y. Segawa, and K. Itami, “Initiation of carbon nanotube growth by well-defined carbon nanorings”, *Nature chemistry* **5**, 572 (2013).
- [30] N. Chen, M. T. Lusk, A. C. T. van Duin, and W. A. Goddard, “Mechanical properties of connected carbon nanorings via molecular dynamics simulation”, *Phys. Rev. B* **72**, 085416 (2005).
- [31] G. Thorner, J.-M. Kiat, C. Bogicevic, and I. Kornev, “Axial hypertoroidal moment in a ferroelectric nanotorus: A way to switch local polarization”, *Phys. Rev. B* **89**, 220103 (2014).
- [32] O. V. Kharissova, M. Garza Castañón, and B. I. Kharisov, “Inorganic nanorings and nanotori: State of the art”, *Journal of Materials Research* **34**, 3998–4010 (2019).
- [33] D. Lehr, R. Alaei, R. Filter, K. Dietrich, T. Siefke, C. Rockstuhl, F. Lederer, E.-B. Kley, and A. Tünnermann, “Plasmonic nanoring fabrication tuned to pitch: Efficient, deterministic, and large scale realization of ultra-small gaps for next generation plasmonic devices”, *Applied Physics Letters* **105**, 143110 (2014).
- [34] H. Omachi, Y. Segawa, and K. Itami, “Synthesis and racemization process of chiral carbon nanorings: A step toward the chemical synthesis of chiral carbon nanotubes”, *Organic letters* **13**, 2480 (2011).
- [35] D. P. DiVincenzo, “The physical implementation of quantum computation”, *Fortschritte der Physik* **48**, 771 (2000).
- [36] D. Leibfried, R. Blatt, C. Monroe, and D. Wineland, “Quantum dynamics of single trapped ions”, *Rev. Mod. Phys.* **75**, 281 (2003).
- [37] J. T. Barreiro, M. Müller, P. Schindler, D. Nigg, T. Monz, M. Chwalla, M. Hennrich, C. F. Roos, P. Zoller, and R. Blatt, “An open-system quantum simulator with trapped ions”, *Nature* **470**, 486 (2011).
- [38] C.-K. Hu, J.-M. Cui, A. C. Santos, Y.-F. Huang, M. S. Sarandy, C.-F. Li, and G.-C. Guo, “Experimental implementation of generalized transitionless quantum driving”, *Opt. Lett.* **43**, 3136 (2018).
- [39] C.-K. Hu, A. C. Santos, J.-M. Cui, Y.-F. Huang, D. O. Soares-Pinto, M. S. Sarandy, C.-F. Li, and G.-C. Guo, “Quantum thermodynamics in adiabatic open systems and its trapped-ion experimental realization”, *npj Quantum Information* **6**, 73 (2020).
- [40] A. Blais, R.-S. Huang, A. Wallraff, S. M. Girvin, and R. J. Schoelkopf, “Cavity quantum electrodynamics for superconducting electrical circuits: An architecture for quantum computation”, *Phys. Rev. A* **69**, 062320 (2004).
- [41] J. Koch, T. M. Yu, J. Gambetta, A. A. Houck, D. I. Schuster, J. Majer, A. Blais, M. H. Devoret, S. M. Girvin, and R. J. Schoelkopf, “Charge-insensitive qubit design derived from the cooper pair box”, *Phys. Rev. A* **76**, 042319 (2007).
- [42] P. Krantz, M. Kjaergaard, F. Yan, T. P. Orlando, S. Gustavsson, and W. D. Oliver, “A quantum engineer’s guide to superconducting qubits”, *Applied Physics Reviews* **6**, 021318 (2019).
- [43] S. Rasmussen, K. Christensen, S. Pedersen, L. Kristensen, T. Bækkegaard, N. Loft, and N. Zinner, “Superconducting circuit companion—an introduction with worked examples”, *PRX Quantum* **2**, 040204 (2021).
- [44] A. C. Santos, “Quantum gates by inverse engineering of a hamiltonian”, *J. Phys. B: At. Mol. Opt. Phys.* **51**, 015501 (2018).
- [45] A. Streltsov, G. Adesso, and M. B. Plenio, “Colloquium: Quantum coherence as a resource”, *Rev. Mod. Phys.* **89**, 041003 (2017).
- [46] M. A. Nielsen, M. R. Dowling, M. Gu, and A. C. Doherty, “Quantum computation as geometry”, *Science* **311**, 1133 (2006).
- [47] X. Fei, V. Hughes, and R. Prigl, “Precision measurement of the magnetic field in terms of the free-proton nmr frequency”, *Nuclear Instruments and Methods in Physics Research Section A: Accelerators, Spectrometers, Detectors and Associated Equipment* **394**, 349 (1997).
- [48] M. Goerbig, “Electronic properties of graphene in a strong magnetic field”, *Reviews of Modern Physics* **83**, 1193 (2011).
- [49] S. Gross, C. Barmet, B. E. Dietrich, D. O. Brunner, T. Schmid, and K. P. Pruessmann, “Dynamic nuclear magnetic resonance field sensing with part-per-trillion resolution”, *Nature communications* **7**, 1 (2016).
- [50] T. Miller, M. Blaskiewicz, R. Boucher, A. Fedotov, D. Gassner, C. Germain, J.-C. Germain, J. Kewisch, M. Minty, S. Seletskiy, H. Song, P. Thieberger, and P. Wanderer, in *6th International Beam Instrumentation Conference* (Grand Rapids, United States, 2017) p. WEPFC05.
- [51] T. Thiele, Y. Lin, M. O. Brown, and C. A. Regal, “Self-calibrating vector atomic magnetometry through microwave polarization reconstruction”, *Phys. Rev. Lett.* **121**, 153202 (2018).
- [52] A. Barenco, C. H. Bennett, R. Cleve, D. P. DiVincenzo, N. Margolus, P. Shor, T. Sleator, J. A. Smolin, and H. Weinfurter, “Elementary gates for quantum computation”, *Phys. Rev. A* **52**, 3457 (1995).
- [53] H.-P. Breuer and F. Petruccione, *The Theory of Open Quantum Systems* (Cambridge University Press, Oxford University Press, Oxford, UK, 2007).
- [54] A. H. Castro Neto, F. Guinea, N. M. R. Peres, K. S. Novoselov,



- and A. K. Geim, “The electronic properties of graphene”, *Rev. Mod. Phys.* **81**, 109 (2009).
- [55] J. L. Mañes, “Symmetry-based approach to electron-phonon interactions in graphene”, *Phys. Rev. B* **76**, 045430 (2007).
- [56] P. Venezuela, M. Lazzeri, and F. Mauri, “Theory of double-resonant raman spectra in graphene: Intensity and line shape of defect-induced and two-phonon bands”, *Phys. Rev. B* **84**, 035433 (2011).
- [57] C.-H. Park, N. Bonini, T. Sohier, G. Samsonidze, B. Kozinsky, M. Calandra, F. Mauri, and N. Marzari, “Electron-phonon interactions and the intrinsic electrical resistivity of graphene”, *Nano letters* **14**, 1113 (2014).
- [58] L. M. Woods and G. D. Mahan, “Electron-phonon effects in graphene and armchair (10,10) single-wall carbon nanotubes”, *Phys. Rev. B* **61**, 10651 (2000).
- [59] T. Sohier, *Electrons and phonons in graphene: electron-phonon coupling, screening and transport in the field effect setup*, *Theses*, Université Pierre et Marie Curie - Paris VI (2015).
- [60] E. H. Hwang and S. Das Sarma, “Surface polar optical phonon interaction induced many-body effects and hot-electron relaxation in graphene”, *Phys. Rev. B* **87**, 115432 (2013).
- [61] M. Pretko and L. Radzihovsky, “Fracton-elasticity duality”, *Phys. Rev. Lett.* **120**, 195301 (2018).
- [62] A. Sedrakyan, A. Sinner, and K. Ziegler, “Deformation of a graphene sheet: Interaction of fermions with phonons”, *Phys. Rev. B* **103**, L201104 (2021).